STUDIES OF HOTSPOT CHARACTERISTICS IN HYBRID X-PINCHES WITH DIFFERENT INTER-ELECTRODE GAPS

A Thesis

Presented to the Faculty of the Graduate School

of Cornell University

in Partial Fulfillment of the Requirements for the Degree of

Master's of Science

by

Jeffrey Hill Musk II

May 2019

ABSTRACT

The hybrid X-pinch configuration for pulsed power experiments consists of a fine wire strung between two solid electrodes, the x-ray burst from which is characterized by a single bright hotspot of soft X-rays under ideal circumstances. These ideal circumstances depend on a number of variables including the size of the gap between the electrodes and the material of the wire used in the test. Testing four different materials (Al, Ti, Mo, Ag) at gap distances ranging from 0.5 to 5.0 mm enabled some insight into the parameters needed to consistently produce a single hotspot. Shots at higher gap distances ($\geq$ 2.0 mm) using the higher-Z materials (Mo, Ag) would produce more hotspots than shots at smaller gap distances ($\leq$ 1.5 mm) with lower-Z materials (Al, Ti). There also appears to be a weak correlation between higher-Z materials and higher energy hotspots, though no such correlation appears for hotspot source size. Understanding the effects of gap distance and wire material on hotspot and X-ray production enables more precise use of the hybrid X-pinch as an X-ray source for spectroscopic studies or backlight imaging.

BIOGRAPHICAL SKETCH

Jeffrey Musk II was born in April 1995 in Seoul, South Korea to Jeff and Misuk Musk. He has two siblings, Kathryn and William, as well as two Boston Terriers, Willi and Waldo. Being in an Army family, Jeffrey spent much of his childhood moving from place to place, spending a majority of his life in either New York or Virginia.

Jeffrey attended the College of William and Mary where he worked towards a B.S. in physics, graduating in 2013. During this time, he began to intern at Sandia National Labs in Albuqeurque. There he began to work in nuclear forensics with Jeff Martin, and would go on to use this work as his thesis at William and Mary with the help of Professor Todd Averett. Jeffrey then began his Master's of Science program at Cornell University in the Applied Engineering Physics department and graduated in May 2019. There he worked in the Laboratory of Plasma Studies (LPS) under Professor David Hammer. After graduating, Jeffrey plans to begin work full time at Sandia National Labs.

ACKNOWLEDGEMENTS

I would like to thank Professor David Hammer for his invaluable guidance as advisor for my research and his services as committee chair. Thanks also to Professor Bruce Kusse for serving as co-chair of my committee. Special thanks to Ahmed Elshafiey, whose work this study is supporting, who helped immensely with running all the experiments and analysis. Thanks as well to Sergei Pikuz and Tania Shelkovenko whose advice and knowledge of hybrid x-pinches was extremely helpful in designing this study. Finally, thanks to the lab technicians at LPS (Todd Blanchard, Dan Hawkes, Billy Potter, Harry Wilhelm) for their support of my experiments. This research was supported by Department of Energy grant number DE-SC0018088 as well as by the National Nuclear Security Administration Stewardship Sciences Academic Programs under Department of Energy Cooperative Agreement DE-NA0003764.

TABLE OF CONTENTS

LIST OF FIGURES

LIST OF TABLES

CHAPTER 1

INTRODUCTION

The hybrid X-pinch is a relatively new wire setup for pulsed power driven plasma experiments. The aim of this experiment was to study the pinch dynamics of different materials when used in the hybrid X-pinch setup.

1.1 Background

The hybrid X-pinch is a combination of the Z-pinch and X-pinch experimental setups. The Z-pinch, or single wire under overwhelming current, is one of the simplest pulsed power experiments in plasma physics. This setup involves a single wire strung along the Z-axis between two flat electrodes that is subjected to a current large enough to cause the wire to explode into a plasma and then to implode to a small radius and emit an intense, short-lived x-ray pulse. Z-pinches have the advantage of being very simple to set up, but are inconsistent in where the plasma micropinches are produced and the accompanying X-ray bursts are formed along the wire.[1, 2, 3]

The X-pinch solves the the Z-pinch's issues with the inconsistent micropinch plasma location by focusing the current at one spot. The simplest X-pinch involves two wires strung between electrodes that cross in an X shape. As there is now a spot along the wires that is subject to more current, the Z-pinch micropinch plasma is more likely to form at the intersection of the wires. While the X-pinch does solve the inconsistent location issues, it is significantly more difficult and time consuming to set up as the angle between the wires must be kept constant between trials. [4, 5, 6]

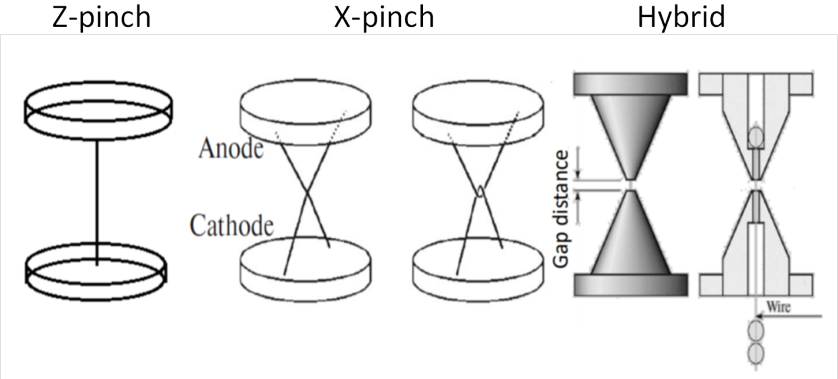

Figure 1.1: Z-pinch, X-pinch, and Hybrid X-pinch Comparisons

A comparison between the wire setups for the Z-pinch, X-pinch, and hybrid X-pinch experiments. An alternate setup in which two wires attached to two electrodes are looped through each other is also shown.

The hybrid X-pinch solves both issues of the Z- and X-pinches. A hybrid X-pinch setup involves a single wire strung between conical electrodes. Having to deal with only one wire makes the set up process much simpler when compared to the standard X-pinch, and by replicating the exploding wire Z-pinch physics in the X-pinch, the hybrid X-pinch does not have the consistency problems of the Z-pinch. Combining the strengths of both setups creates an appealing design for diagnostics or repeated measurements, as it enables both a simple setup and consistent results. As the hybrid X-pinch is a somewhat recent development in the world of exploding wire experiments, its dynamics are not fully understood. This study investigated how different wire materials and the position of the electrodes affect how the hybrid X-pinch produces hotspot plasma events. [7, 8, 11]

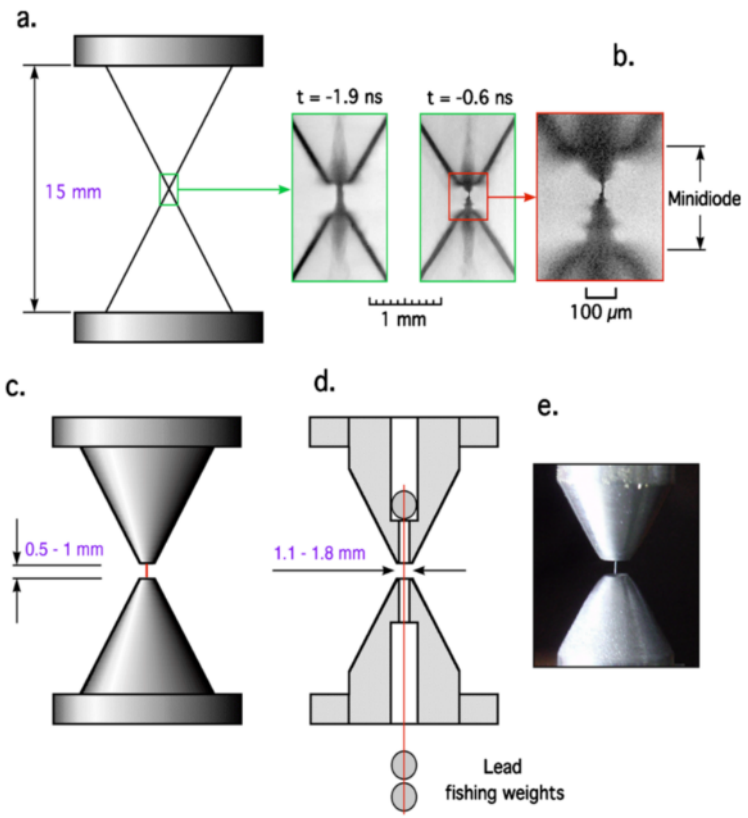

Figure 1.2: X-pinch and Hybrid X-pinch Minidiode Dynamics

A look at how the traditional X-pinch develops in time and how the hybrid X-pinch setup looks to emulate that development in its initial position. The area of interest (boxed in red) is about 0.5 mm long. A 0.5 mm electrode gap distance will be tested using the hybrid X-pinch setup. [7]

1.2 Literature

The concept of the hybrid X-pinch was first published in a 2010 paper titled *Hybrid X-pinch with conical electrodes* by Doctors Tania Shelkovenko and Sergei Pikuz. This study was performed in a collaboration between the Laboratory of Plasma Studies at Cornell University, Sandia National Labs, and the P.N. Lebedev Physical Institute in Moscow, Russia. The paper details the new concept of the hybrid X-pinch and outlines how the hybrid setup imitates the traditional X-pinch setup. [7]

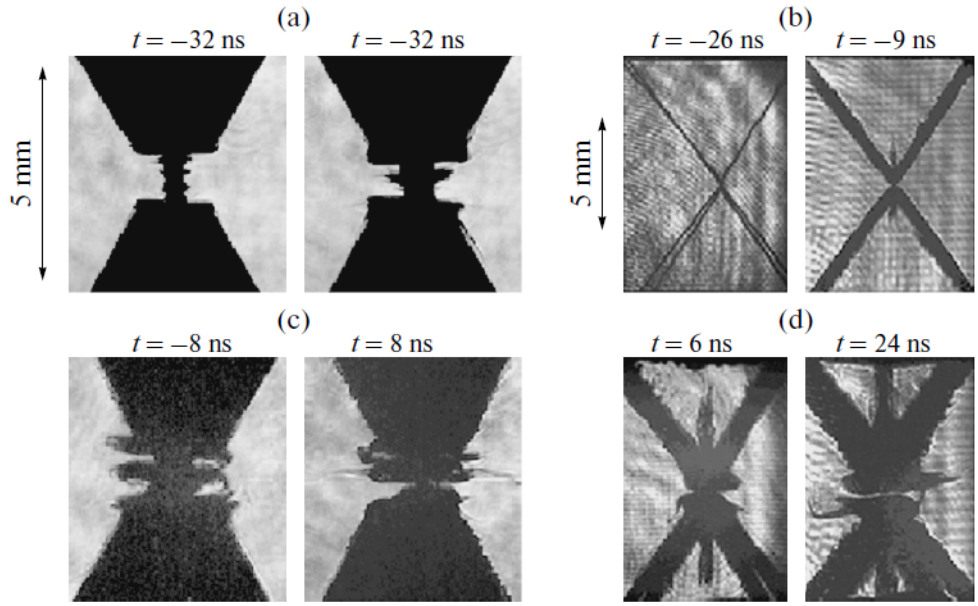

Figure 1.3: Early stages of development in X-pinches and Hybrid X-pinches

A comparison between how the hybrid x-pinch (a, c) and traditional x-pinch (b, d) develop in time for aluminum wires. Shown are the two distinct early stage setups (a, b) and the similar final stages (c, d). [11]

Hybrid X-pinch with conical electrodes describes the traditional X-pinch as consisting of "two or more fine wires that cross at a point as a load of a 100-500 kA pulsed power generator." The most important processes of the traditional X-pinch take place in a 1 mm region surrounding the intersection of the two wires. During the initial development of the X-pinch, a dense mini-diode is formed from the wire material produced in the wire explosion (see figure 1.2a). These dense plasma "electrodes" are connected by a column of plasma created during the explosion of the wire that goes on to implode and create a hotspot and X-ray burst. The plasma and resulting X-rays are the important factors to consider when attempting to replicate results with a new setup. [7, 8, 9, 10]

This minidiode phenomena is explored in more detail in the 2014 paper *Dynamics of Hybrid X-Pinches*. Several laser shadowgraphs of hybrid x-pinch tests

are presented to illustrate how the setup evolves with time. In particular, a comparison between the development of the hybrid and standard X-pinches is presented as seen in figure 1.3. The similarities between the two setups can be seen in the final stages of development. As only a small percentage of the ions reach the diode gap, the final compression for both X-pinches "differ insignificantly". [11]

As stated previously, the traditional X-pinch loading process is both inconsistent and time-consuming. Great care must be taken to cross two fine wires, typically less than 100 μm thick, at certain angles with relative consistency, in order to have the wires break down into dense mini-diodes connected by a plasma column. Thus, creating artificial diodes that act similarly to the mini-diodes is an attractive solution that enables a much simpler and more predictable set up process. Assuming the damage to the solid diode electrodes is minimal, only the wire would have to be replaced before the next shot is performed. [7, 8]

The *Hybrid X-pinch* paper then goes into detail about an important phenomenon regarding the electrodes and production of the plasma hotspot. During the wire explosion, intense UV radiation produces a plasma on the surface of the electrodes that moves into the diode gap. If an X-pinch hotspot has not formed by the time these two plasmas meet in the middle of the gap, the normal X-pinch process is interrupted. The time, t_{hs}, before which the hotspot must form before the diode gap is closed is roughly:

$$t_{hs} = t_0 + \frac{d}{2v_p} \tag{1.1}$$

where $v_p \approx 10^6$ cm/s is the velocity at which the plasma on the electrodes ex-

pands, t_0 is the time between the start of the current and plasma formation, and d is the gap distance between the two electrodes. The time t_0 depends on the current rise time and is around 15 ns. So one way to increase the gap closure time is to expand d. This comes with the risk of a gap distance large enough that multiple hotspots and X-ray bursts form. It is this variable, d, that this study is designed to understand. [7]

In their 2015 papers *X-Pinch. Part I* and *X-Pinch. Part II*, Shelkovenko and Pikuz reaffirm the benefits and uses for the hybrid setup. In *X-Pinch. Part I*, the hybrid X-pinch is used in both mega-ampere and lower current X-pinch machines. The paper then goes on to highlight that despite the vastly different wire setup, the hybrid X-pinch development takes place "according to similar scenarios and, in the final stage, leads to the formation of [hotspots] with similar parameters" when compared to the traditional X-pinch. *X-Pinch. Part II* details several features of the hybrid X-pinch that give it an advantage over the traditional design. According to *Part II*, the hybrid X-pinch produces smaller radiative regions and achieves a shorter time delay between the soft X-ray and hard X-ray peaks. The hybrid setup also enables studying spectra for almost any element where such a feat was not possible with the traditional setup. [12, 13]

1.3 Goals

The end goal of this experiment is to determine if there is a specific setup for the hybrid X-pinch that will produce a single bright hotspot (bright X-ray emission point) with relative consistency. Searching for this setup will involve testing different materials and different electrode gap distances. Testing different gap

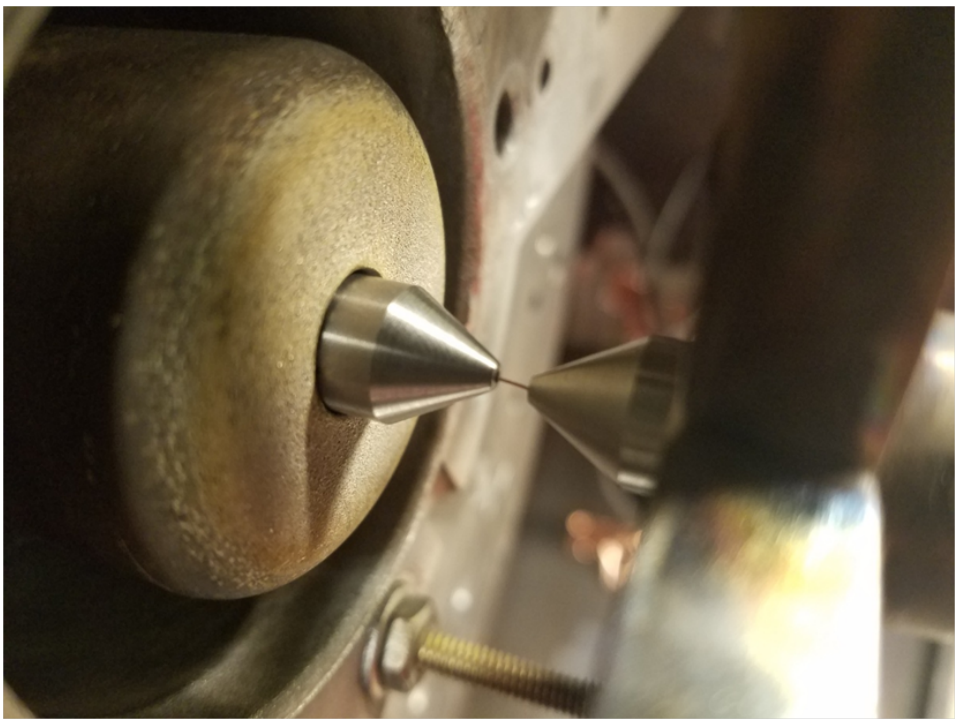

Figure 1.4: Electrode Gap Distance

An image showing the gap distance between the two electrodes that is being studied. Gap distances are set using a leafing gauge to precisely set the location of the electrodes.

distances affirms that larger electrode gap distances leads to more hotspots being produced, as anticipated. Testing these materials will also provide valuable insight into whether or not hotspot production scales with electrode gap distance differently for the different materials. Finding a setup for each material that produces a single hotspot makes study of the plasma created much simpler as multiple hotspots can overlap and interfere with each other.

Study of the hotspots will also reveal information about the X-ray energy and the size of the plasma source. In general, a plasma hotspot that produces a bright soft X-ray source while being around 1 μm in diameter is a good plasma event. This investigation will look for the relationship between material and source size, number of hotspots, and X-ray energy.

This study is working towards a larger study investigating radiative collapse. Radiative collapse is a process that occurs when the current exceeds a critical value, I_c, causing the magnetic field to decrease the size of the plasma spot and increase its density. This then causes the radiation rate to increase, cooling the plasma and reducing the plasma pressure faster than ohmic heating and radial compression are increasing it. Observation of this phenomena requires both picosecond resolution and time-integrated X-ray spectroscopy. The ability to produce a consistent single hotspot helps in timing an X-ray streak camera to view such a narrow window. Multiple hotspots can also interfere with each other, increasing the difficulty of observing radiative collapse. [14, 15, 16]

CHAPTER 2

METHODS

2.1 Experimental Process

The bulk of the experiment revolved around firing the X-pinch Machine (XP) at a range of gap distances for different materials. Based on previous experiments with silver wire, the target gap distance studied was between 1.0-3.0 mm at 0.5 mm intervals. A few shots outside this range were taken to determine if trends continue in the extreme cases (0.5, 4.0, and 5.0 mm). At five shots for each gap distance in the target interval and three shots for each extreme case, the total number came to 136.

The wire materials to be studied were aluminum, titanium, molybdenum, and silver. Silver has been proven to be a high consistency material for hybrid x-pinches. Aluminum, molybdenum, and titanium are to be used in the radiative collapse study. This selection of materials also provides a mix of high-Z and low-Z materials.

Material	Z-number	Diameter	Mass per length (g/m)
Aluminum	13	66	1.176×10^{-2}
Titanium	22	50	1.125×10^{-2}
Molybdenum	42	30	0.925×10^{-2}
Silver	47	33	1.143×10^{-2}

Table 2.1: Table of Hybrid X-pinch Materials and Properties

A table of the materials used for the shots in the hybrid x-pinch experiments. The diameters were chose to keep mass per length relatively constant. This gives some insight into how the materials behave differently based on Z-number rather than total mass.

Figure 2.1: XP Machine

A picture of the XP machine in the LPS lab in Grumman Hall. The capacitors are stored in oil in the yellow tank at the back. The middle tank holds the ISC and PFL submerged in water. The front chamber houses the wire load and many diagnostics (see figure 2.2).

2.1.1 XP Machine

The experiment was carried out on the XP Machine (X-Pinch Machine). XP consists of a Marx Generator, a water tank containing an Intermediate Storage Capacitor (ISC) and Pulse Forming Line (PFL), and a vacuum chamber. In the Marx Generator, multiple capacitors are charged in parallel then discharged in series. In this experiment, the discharge voltage was set to be 38 kV. The current pulse then moves through the ISC and PFL, and is finally discharged through the load wire. The peak current for the machine is around 300 kA with a rise time of 50 ns.

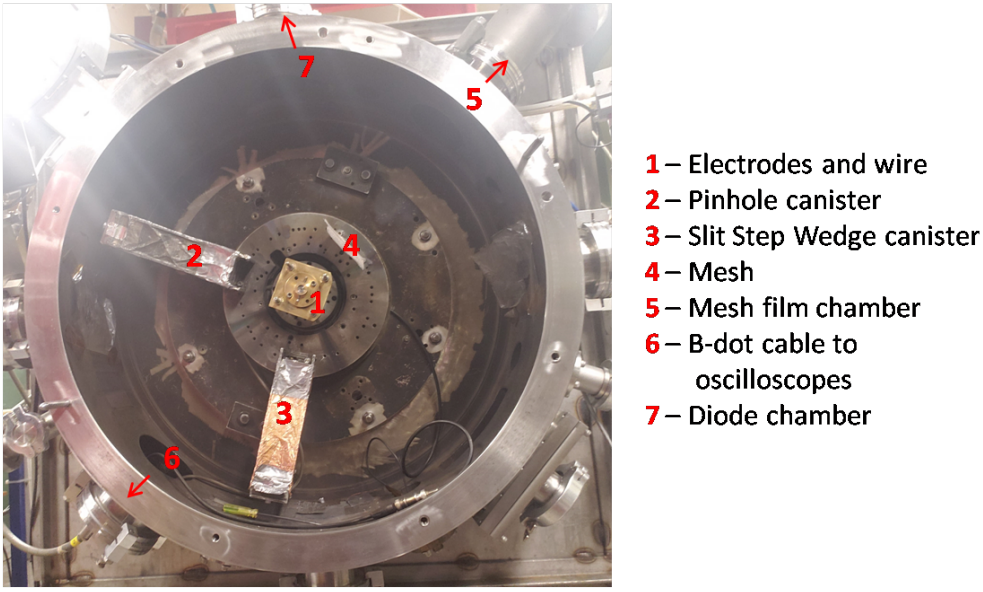

Figure 2.2: XP Machine Diagnostic Chamber

The vacuum chamber in which the electrodes, wire, and many diagnostics are loaded. The film canisters are removed between each shot to scan image plates or develop film. The electrodes are either polished or replaced between shots to minimize surface damage that could affect the results of the shot.

2.2 Diagnostics

The main variable recorded was the number of hotspots produced for each shot. X-ray energy as measured by fitered PCDs, source size, and XP current and rise time were recorded as well. This was accomplished using a combination of image plates in film canisters and oscilloscopes.

2.2.1 Image Plates, Film, and Canisters

The image plates used to determine properties of the hotspots are Fujifilm BAS-SR 2025 imaging plates. These imaging plates utilize photostimulated luminescence to record X-ray signatures from the hotspots generated by the hybrid

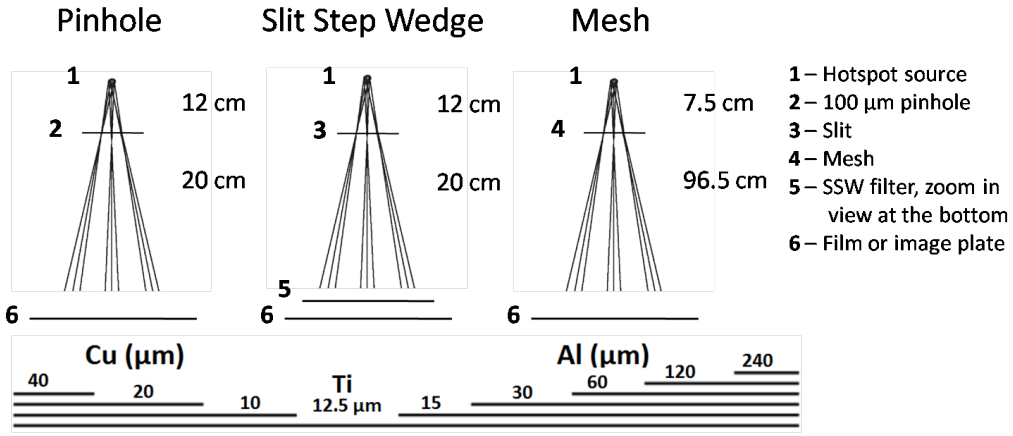

Figure 2.3: Pinhole, SSW, and Mesh Diagrams

Diagrams of setups of the two film canisters, the pinhole and SSW, as well as the mesh setup. As seen in figure 2.2, the mesh is not contained in a canister. Instead, the mesh is held close to the electrodes while the film is held in a tube extending about a meter out from the chamber. The bottom diagram shows the construction of the SSW (slit step wedge) filter.[18]

x-pinch. The plate consists of a layer of photostimulable phosphor that stores energy from the X-rays to record the image. The plates then emit light proportional to the energy stored when exposed to a laser. With use of a laser scanner, the X-ray images can be stored for later use. [17]

The films and image plates are loaded into film canisters, which are placed in the vacuum chamber facing the hybrid x-pinch between the electrodes. These canisters are 20 cm in length with a slit or hole at the top to view the hotspot and a slot for the films at the bottom (see figure 2.3). By placing the top of the canisters 10 cm away from the electrodes, the films achieve a magnification of 3, according to the formula:

$$M = \frac{(a+b)}{a} \tag{2.1}$$

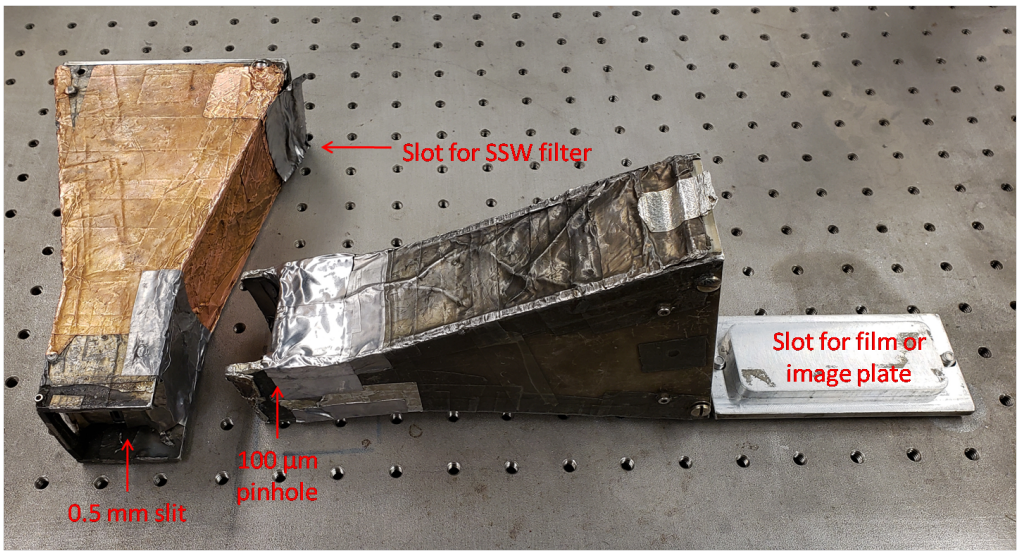

Figure 2.4: Film Canisters

The canisters in which the image plates or film are loaded. Both canisters have the same dimensions. The left canister is used for SSW images while the right is used for pinhole. [18]

where a is the distance to from the source to the canister and b is the length of the canister.

For better resolution, Kodak Industrex DR50 film were used for imaging the mesh. The DR50 film is a fine grain film designed to deliver high contrast when exposed to high voltage X-rays. After being developed, the film is scanned into the computer at 2650 dpi (dots per inch). DR50 film was used to record high resolution images for use in calculating the hotspot source size. [19]

2.2.2 Pinhole

The pinhole camera filter was one of the two film canisters looking at the hotspot. This canister has a 100 μm hole at the top to image the hotspot. This image is used to view the position and relative intensity of the hotspots in relation

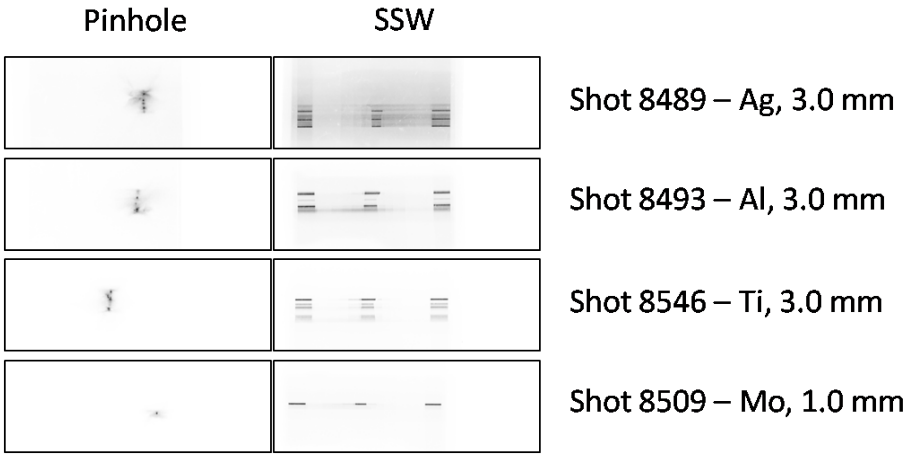

Figure 2.5: Pinhole and SSW Output Images

Examples of images generated from the pinhole and SSW film canisters. These pictures are scanned off the image plates and are mainly used to view the number of hotspots generated.

to the wire and the two electrodes.

2.2.3 Slit Step Wedge

The slit step wedge filter was used with an image plate to both count the number of hotspots generated and give an idea of the energy range of the X-rays. X-rays travel through a 0.5 mm slit at the top of the film canister and are attenuated in a set of filters that is placed directly above the image plate. The filter consists of multiple layers of copper, titanium, and aluminum (see figure 2.3), each of which filters out different energies of X-rays enabling a preliminary analysis of the intensity of the hotspot before more in depth calculations are performed based on readings from the photoconducting diodes.

Images from the slit step wedge were also used to calculate the hotspot source size. By taking an intensity profile of the slit step wedge (SSW) camera

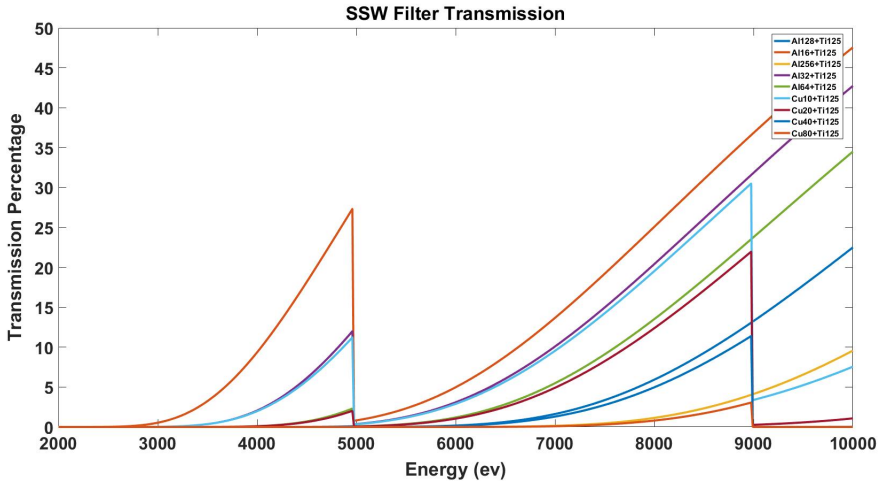

Figure 2.6: Plot of SSW Transmission Lines

A plot of the energy transmission through the layered filters of the SSW. As seen in figure 2.3, the filters are thinnest at the center. Thus a wider image generated corresponds to a higher energy hotspot.[22]

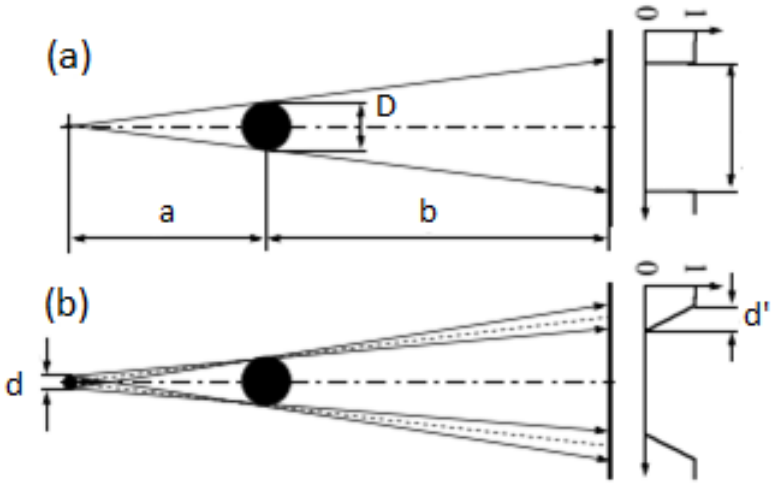

Figure 2.7: Diagram of Source Size Calculation

A diagram showing the process of calculating the source size and the difference between an ideal point source and the experimental hotspots. The penumbra are measured by scanning the film into an image processing software and plotting the intensity of the image (intensity vs. pixels). The pixel values on the intensity plot can then be converted to a distance for use in source size calculations. [21]

images, we measure the width of the line images created by the X-rays through the slit. Because the hotspot is not a true point source, there will be small transition regions, or fringes, on the edges of the width (see figure 2.6). The source size d is calculated using the equation:

$$d' = \frac{b}{a}d \tag{2.2}$$

where d' is the width of the penumbra, a is the distance from the hotspot to the slit, and b is the distance from the slit to the image plate. Using the magnification, we verify the width of the slit to ensure the calculations were correct.[20]

2.2.4 Mesh

Similarly to the slit step wedge camera, a mesh is also used to calculate the source size. In this setup, a 10 cm $\times$ 10 cm mesh is placed between the hotspot source and a film. The mesh is made of 75 μm wire and has 7 squares per cm. By placing the mesh closer to the electrodes and the film farther away, the recorded image has a greater magnification than possible with the film canisters, enabling more accurate source size calculations. Equation 2.2 is still used, substituting in the distance from the source to the mesh for a and the distance from the mesh to the film for b. The setup used had $a = 8.89$ cm and $b = 96.52$ cm for a magnification of $M = 11.85$. Images of the mesh will be recorded on the DR50 film so as to ensure the best possible resolution for source size calculations.

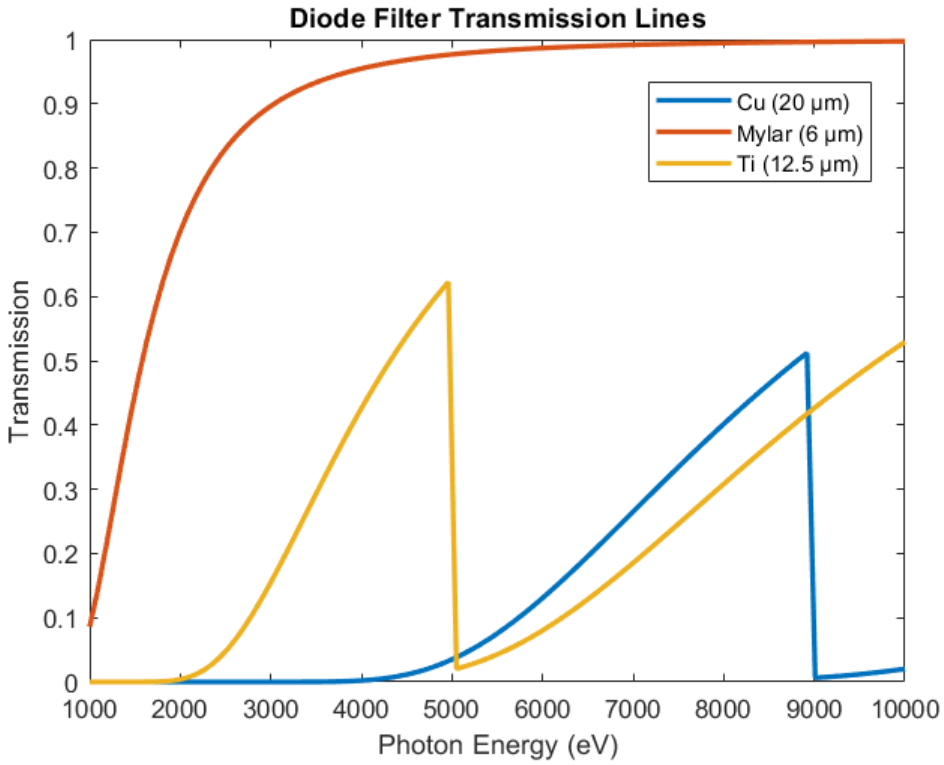

Figure 2.8: Plot of PCD Filter Transmission Lines

A plot of the transmission lines for each diode filter as a function of the photon energy. The variation in filter transmissions enable insight into different energy regimes.[22]

2.2.5 Diodes

Three diodes with different filters are used to record the energy of the X-rays from the hotspots. The three filters used were 20 μm copper, 12.5 μm titanium, and 6 μm mylar. Each filter looks at a certain energy range, 2-5 keV for Ti, 4-9 keV for Cu, and 1-10 keV for mylar. These energy ranges can be seen in figure 2.7. [22, 23]

Readings from the diodes are used to calculate the energy from photons in the given range generated by the hotspot using the following equation:

$$E_d = \frac{\int V dt}{R\psi_d} S_f \tag{2.3}$$

where V is the voltage reading from the diode, R is the internal resistance of 50 Ω, ψ_d is the sensitivity of the diode, and S_f is a geometrical factor based on the surface area of the diode. This geometric factor is based on the assumption that radiation given off by the hotspot is spherically symmetric. The diode then measures a small section, A_d, i.e., the diode surface area, of the surface area, A_c, irradiated. This factor is given by:

$$S_f = \frac{A_c}{A_d} = \frac{4\pi r_c^2}{l_d w_d} \tag{2.4}$$

where r_c is the distance from the hotspot source to the diodes and r_d is the radius of the diode. These values come out to be $r_c = 70$ cm, $l_d = 3$ mm, and $w_d = 1$ mm giving a value of $S_f = 2.18 \times 10^5$ for the geometric factor.

2.2.6 Current Traces

Current trace waveforms from the XP machine are connected by double shielded 50 ohm coaxial cables to three oscilloscopes in an electromagnetically shielded diagnostic room (”Faraday cage”). The oscilloscopes record the shape of the voltage in the ISC and PFL using capacitive voltage dividers, and the time-derivative of the current through the load using a B-dot probe. Traces from the three scopes are fed into a computer using LabVIEW. The LabVIEW program then integrates the signal from the B-dot using Python to give the ac-

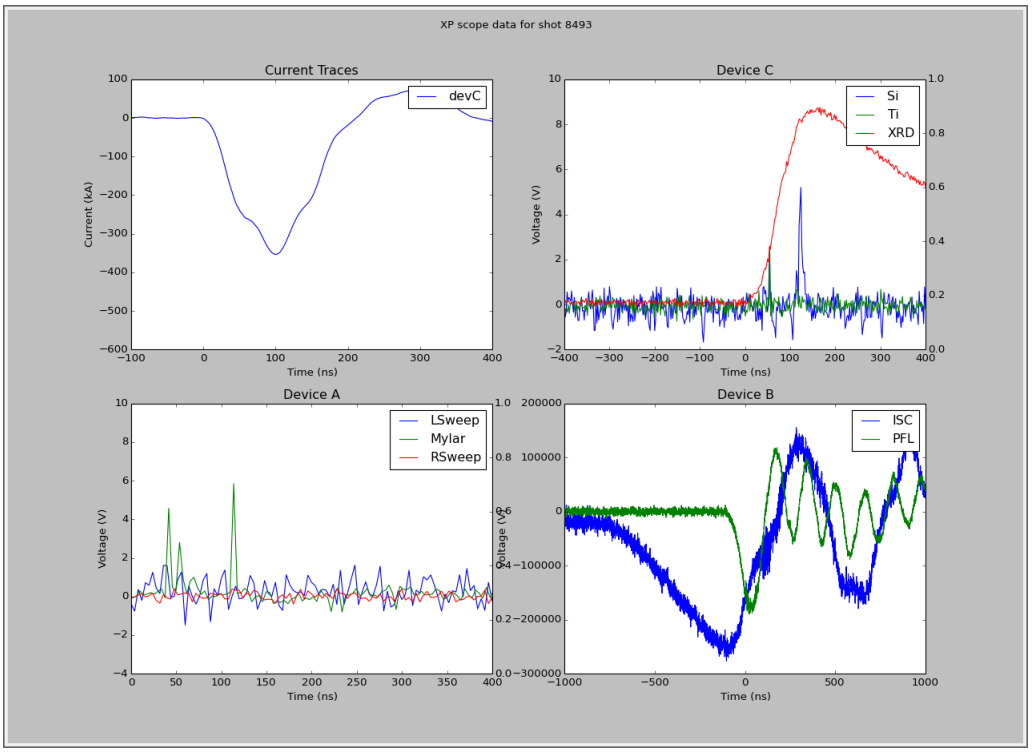

Figure 2.9: XP Machine Output Traces

An example of the scope traces showing the current (top left), diode (top right, bottom left), and PFL/ISC readings (bottom right). The current and PFL/ISC traces should remain constant between shots.

tual current travelling through the load. This load current and signals from the PCDs, ISC, PFL are plotted together to make it easy to check if everything about the shot appears to be as expected.

An important part of being able to use the oscilloscopes accurately is accounting for cabling delays between the different signals. This process involves measuring the length of the cables that run from the sources on the XP Machine to the scopes as well as a few cables that run between scopes. Each meter of wire corresponds to about 5 ns of delay. By taking into account the delay in LabVIEW, the graphs seen in figure 2.9 will be spaced correctly.

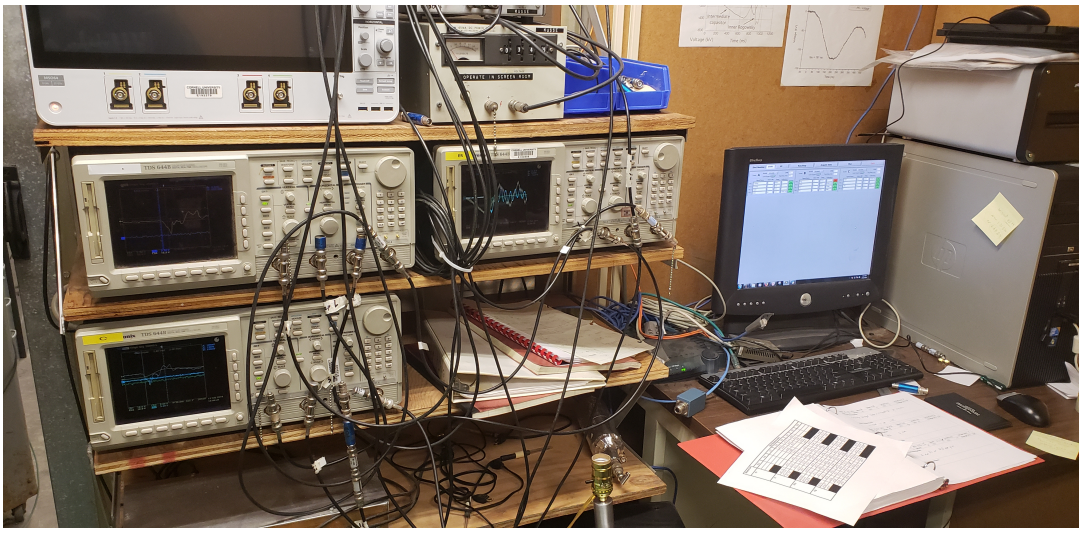

Figure 2.10: XP Machine Trace Room

The three scopes and computer running LabVIEW that are used to record the current and diode traces from the XP shots. The whole setup is contained in a Faraday cage room to protect the oscilloscopes from noise signals from XP.

Magnetic B-Dot Probe

A B-Dot probe is used in the vacuum chamber to measure the rate of change of the magnetic field with time ($\dot{\mathbf{B}}$). This loop of wire encircles the load to measure the current that is applied to the fine wire between the two electrodes. By Faraday's Law ($\nabla \times \mathbf{E} = -\frac{\partial \mathbf{B}}{\partial t}$), the changing magnetic field created by the current in the load induces an electric field. This electric field is recorded as voltage and sent to the oscilloscopes. Knowing the magnetic field enables calculation of the current by way of Ampere's Law ($\oint \mathbf{B} \cdot d\mathbf{l} = \mu_0 I_{enc}$).

CHAPTER 3

RESULTS

Data collection began on December 14, 2018 and was completed on February 18, 2019 (Shots 8432-8607). During this time, data for the 136 shots was taken without any issues from the XP machine with the only delay coming from a shortage of aluminum wire. The number of hotspots for each shot was determined by the slit step wedge images, a few examples of which can be seen below. An extra series of shots (8619-8630) was taken from March 19-22, 2019 for source size calculations using a mesh. These shots were not taken into account for the averages seen in the plots below. Tables detailing hotspots generated for each shot can be found in the appendices.

3.1 Aluminum Series

Hotspots for aluminum appear to act as a step function with respect to the electrode gap distance. In the 0.5-1.5 mm range, all shots produced either 1 or 2 hotspots for a total average of 1.38. Shots taken at 2.0 or 2.5 mm also acted similarly to each other, all producing 2 to 4 hotspots with a total average of 3.1. For 3.0 and 4.0 mm, shots produced 4-6 hotspots for a total average of 4.86. Shots at 5.0 mm produced between 5 and 8 hotspots for an average of 6.33. A plot of these data can be seen in figure 3.1.

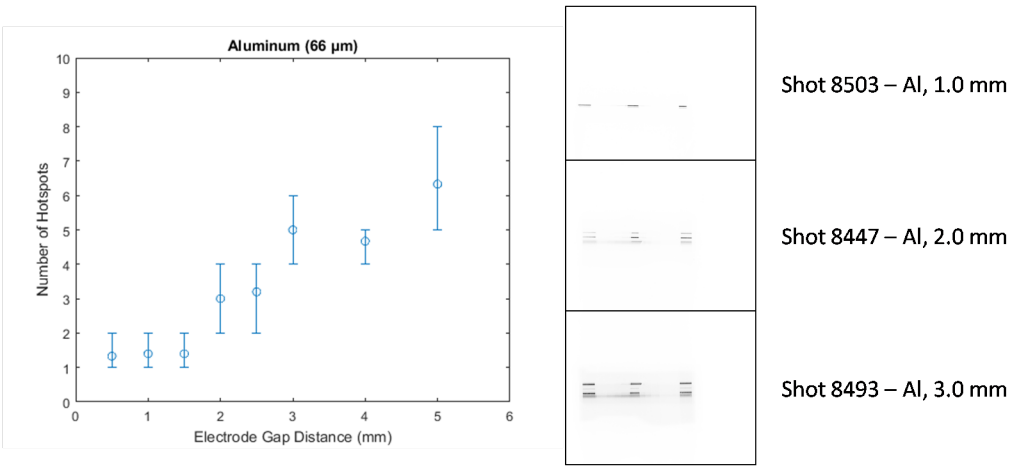

Figure 3.1: Plot of Aluminum Series Results

A plot of the average number of hotspots for aluminum with the error bars indicating the maximum and minimum number of hotspots. Example SSW images for three different gap distances are also included.

3.2 Titanium Series

Hotspots generated using titanium wire appeared to follow a simple linear trend. Unlike aluminum where the average would remain relatively constant for a few gap distances, titanium shots displayed a steady increase in the average number of hotspots generated as the electrode gap distance was widened. Most gap distances had a spread of 1 or 2 hotspots generated. Only the series at 2.5 and 5.0 mm displayed shots with a spread of 3 between its minimum and maximum number of hotspots. A plot of these data can be seen in figure 3.2.

3.3 Molybdenum Series

Much like titanium, the average number of hotspots generated by a molybdenum shot increases in a largely linear fashion. However unlike titanium, the

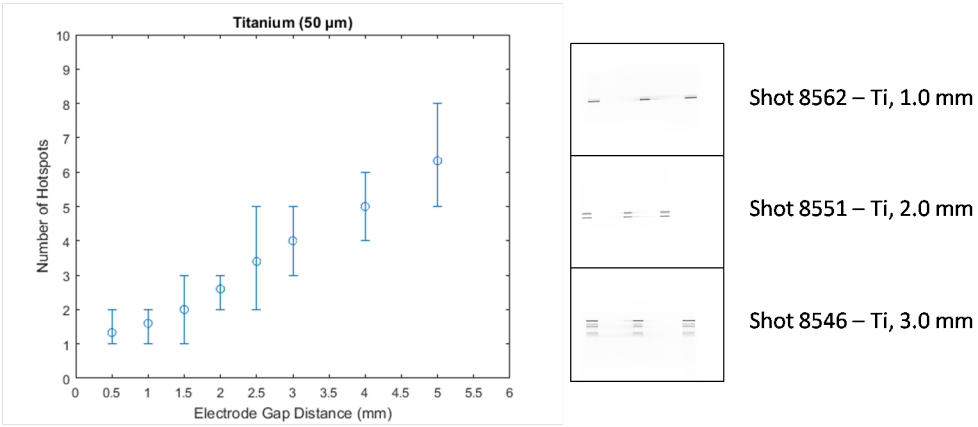

Figure 3.2: Plot of Titanium Series Results

A plot of the average number of hotspots for titanium with the error bars indicating the maximum and minimum number of hotspots. Example SSW images for three different gap distances are also included.

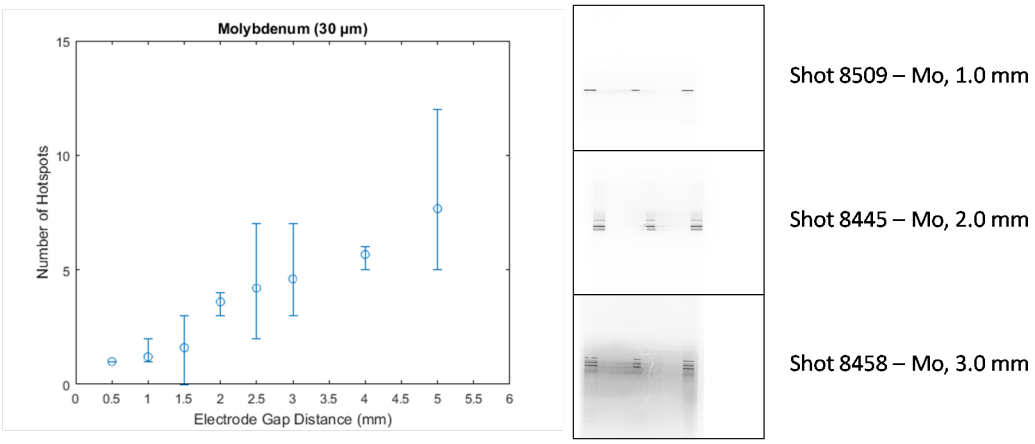

Figure 3.3: Plot of Molybdenum Series Results

A plot of the average number of hotspots for molybdenum with the error bars indicating the maximum and minimum number of hotspots. Example SSW images for three different gap distances are also included.

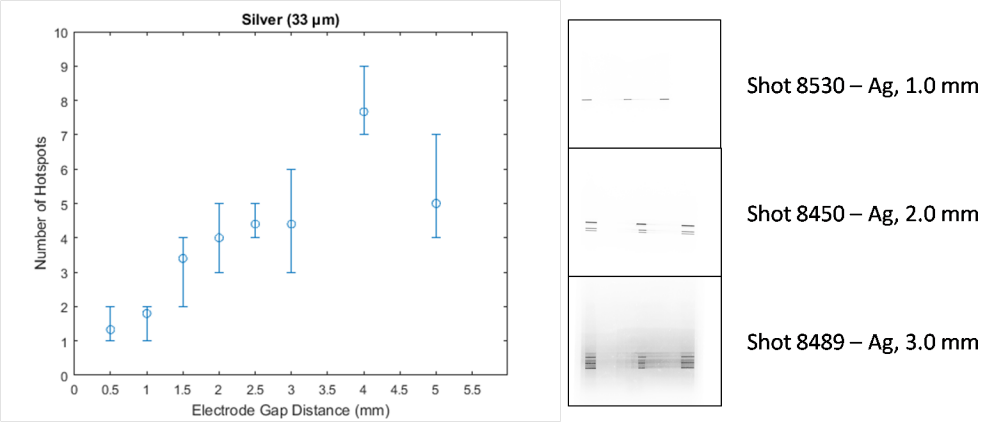

Figure 3.4: Plot of Silver Series Results

A plot of the average number of hotspots for silver with the error bars indicating the maximum and minimum number of hotspots. Example SSW images for three different gap distances are also included.

spread of hotspots for molybdenum is less uniform across different electrode gap distances. The smallest spread is 0 at 0.5 mm while the largest spread is 7 at 5.0 mm. There seems to be no trend in the spread, as the series at 1.0, 2.0, and 4.0 mm had a spread of 1 while those at 1.5, 2.5, and 3.0 had larger spreads. A plot of these data can be seen in figure 3.3.

3.4 Silver Series

Hotspots generated by silver shots do not follow a linear trend as cleanly as titanium or molybdenum. The series of shots taken at 4.0 mm appears to be an outlier when compared to the trend of the other gap distances. The series of shots at 2.5 and 3.0 mm produced the same average number of hotspots, likely due to the difference in spread. The spread for any given gap distance ranges between 1 and 3, with both series at 0.5 and 1.0 mm having spreads of 1. A plot of these data can be seen in figure 3.4. In both the molybdenum and silver

3.0 mm SSW images, the lines indicating the hotspots are surrounded by a grey shading. This shading is due to electron beam radiation due to the higher Z of these materials. [18]

3.5 Mesh Series

A series of twelve extra shots was taken adding the mesh setup detailed in section 2.2.4. These shots were used for source size calculations and were not taken into account in the plots and averages seen above. However, these shots do seem to follow the trends from the original series. All shots were taken at 0.5 or 1.0 mm to attempt to produce a single hotspot. Of the twelve shots, eight produced a single hotspot while the other four produced two. This is in line with the larger series of shots taken at 0.5 and 1.0 mm. A table of these shots can be seen in appendix A.1.5.

CHAPTER 4

ANALYSIS

Armed with data from the slit step wedge filter, diodes, and pinhole, we can analyze the dependence of the hotspot and energy on the electrode gap distance. The slit step wedge and pinhole were used to count the hotspots produced for each shot. Readings from the diodes and equations 2.2-3 will be used to calculate the energy.

4.1 Number of Hotspots vs. Electrode Gap Distance

All materials follow the same general trend of a larger electrode gap distance producing more hotspots. The larger gap distance presents more space along the wire for hotspots to form along the wire, which leads to an average of 6.04 hotspots for shots at 4.0 and 5.0 mm. Shots in this range had a spread of 8, ranging between 4 and 12 hotspots over all materials.

On the other end of the spectrum, shots at 0.5 and 1.0 mm produced 1.41 hotspots on average. All shots in this range produced either 1 or 2 hotspots for a spread of just 1. This consistency is promising for experiments that require a single X-ray source.

How the hotspots scale up with electrode gap distance varies between materials. Titanium and molybdenum hotspots each scale very linearly, with coefficients of determination of $R^2_{Ti} = 0.992$ and $R^2_{Mo} = 0.967$. Aluminum also has strong linear scaling, though less so than titanium and molybdenum with $R^2_{Al} = 0.915$. In a vacuum, you could say that silver scales linearly, but compared to the other three its linear scaling is much weaker at $R^2_{Ag} = 0.692$ Linear fits of

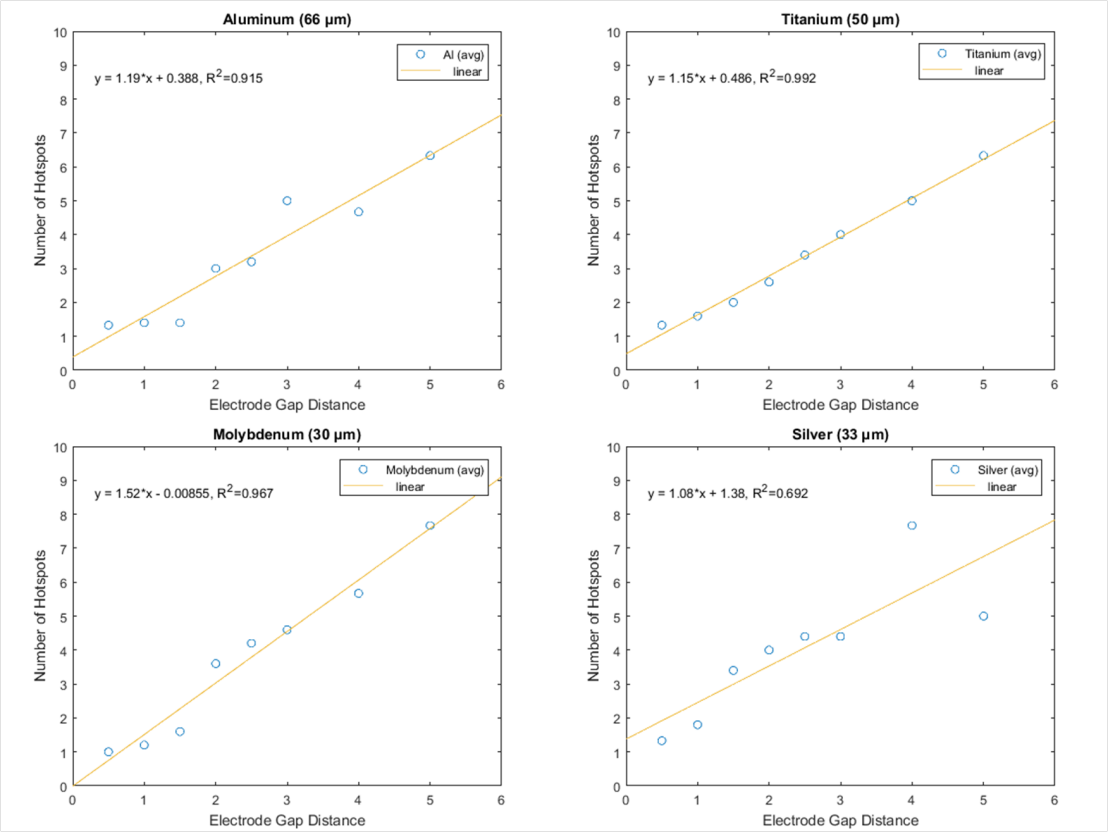

Figure 4.1: Plots of Linear Fits of Average Hotspots

Plots of all four materials with linear fits. Titanium and molybdenum have strong linear progression, aluminum slightly less so, and silver has somewhat weak linear progression.

all materials' data sets can be seen in figure 4.1.

While aluminum does have strong linear scaling ($R^2_{Al} = 0.915$), a different possibility for a fit is a stepwise function. Unlike titanium and molybdenum where each increasing gap distance corresponds to a higher average number of hotspots, adjacent aluminum gap distances hold more constant. By taking the average number of hotspots for electrode gap distances that act similarly (0.5-1.5, 2.0-2.5, 3.0-4.0, 5.0) we can construct a reasonable stepwise fit. As there is no way to measure the goodness of a stepwise fit, an eye-test is the best we can to. A stepwise fit along with the aluminum data can be seen in figure 4.2.

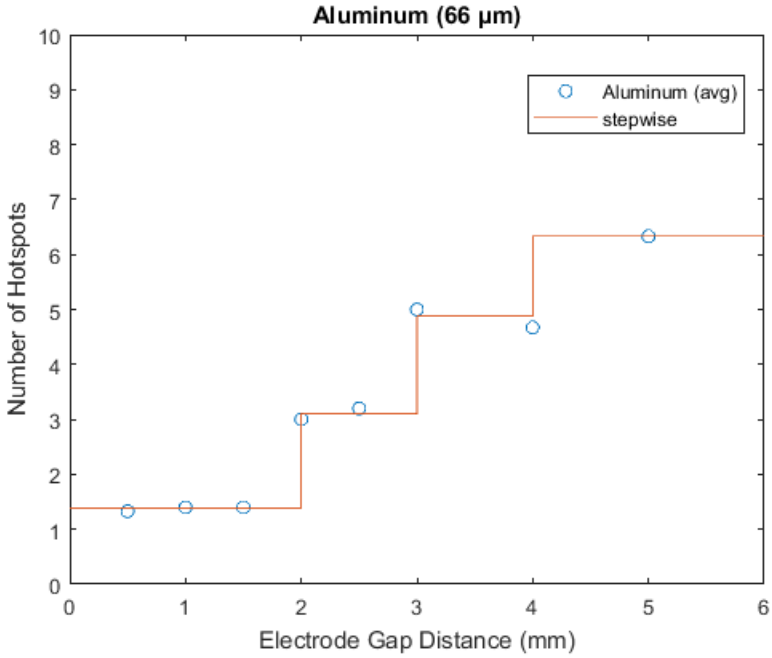

Figure 4.2: Stepwise Plot of Aluminum Hotspots

Aluminum hotspot data along with a stepwise fit based on the average number of hotspots for adjacent gap distances. Since adjacent gap distance have similar averages, the aluminum data seems to fit the stepwise function very well.

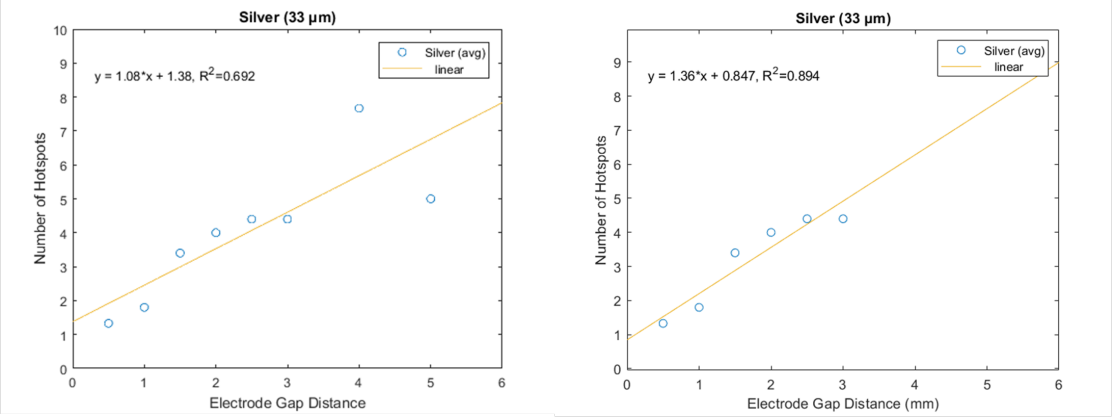

Figure 4.3: Plots of Silver Hotspots with and without Outliers

A comparison between a linear fit of the un-edited silver hotspot data and a fit that removes the 4.0 and 5.0 mm points. Removing what appears to be an outlier, the linear goodness of fit does significantly improve ($R^2_{Ag} = 0.692 \rightarrow R^2_{Ag} = 0.894$). The data appears to level out as gap distance increases, but this does not seem realistic given the results from the other materials.

Silver acts as a bit of an anomaly. It's linear scaling is much worse than the other three ($R^2_{Ag} = 0.692$ vs. $R^2_{Ti} = 0.992, R^2_{Mo} = 0.967, R^2_{Al} = 0.915$), and it doesn't appear to follow the same stepwise characteristics as aluminum. Removing what looks like outliers at 4.0 and 5.0 mm does significantly improve the fit ($R^2_{Ag} = 0.692 \rightarrow R^2_{Ag} = 0.894$). Based on the trend from the lower gap distances (0.5-3.0 mm), the series of shots at 4.0 mm produced more hotspots than expected while the series at 5.0 produced less. This indicates that at higher gap distances, shots using silver wire are more volatile and less predictable in their hotspot production. A plot without the outliers can be seen in figure 4.3.

Analyzing differences between the average number of hotspots at each electrode gap distance does appears to show a slight trends between the materials. The two heavier materials, molybdenum and silver, produced the most hotspots for 7/8 gap distances. Silver produced the most hotspots for 6/8 gap distances and molybdenum produced the second most for 5/8 gap distances. On the other end, aluminum and titanium produced the least hotspots for 5/8 gap distances. This leads to a slight trend that higher-Z materials leads to more hotspots when under the same conditions as a lower-Z material.

4.2 Energy vs. Electrode Gap Distance

Each of the three filters on the photoconducting diodes give insight into the energy generated. This section looks into the differences in energy emission for each hybrid x-pinch material and gap distance. Energy readings are based on the most intense hotspot for each shot with no attenuation on the oscilloscope readings.

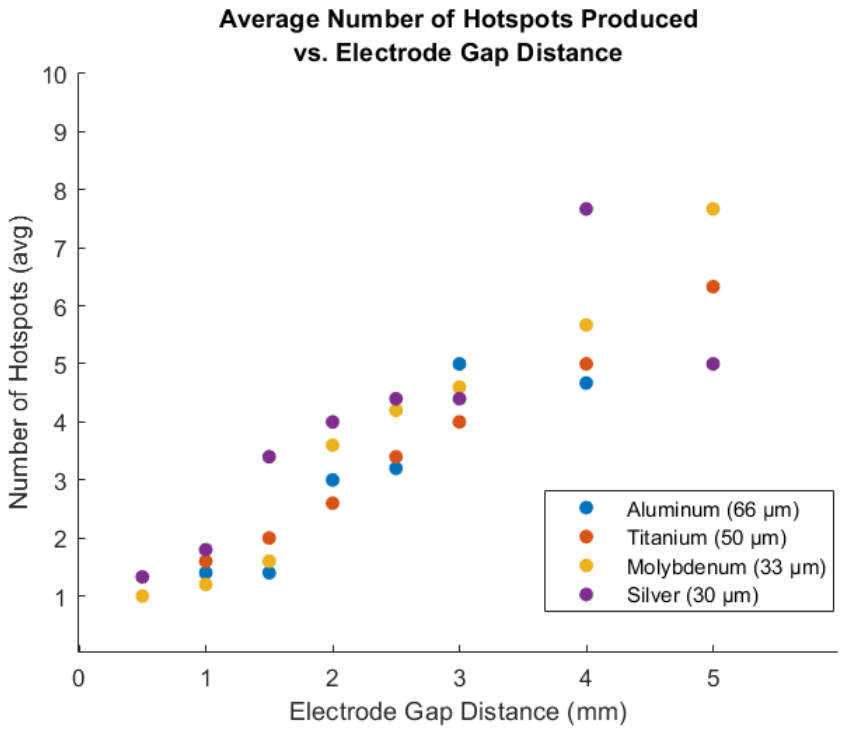

Figure 4.4: Plot of Average Hotspots across all Materials

A plot of the average number of hotspots produced against electrode gap distance for all four materials. A few averages overlap at 0.5 and 5.0 mm ($Al_{avg,1.5} = Ti_{avg,1.5} = Ag_{avg,1.5} = 1.33$ and $Al_{avg,1.5} = Ti_{avg,1.5} = 6.33$). When all the data is presented, there is a clear upward trend for number of hotspots vs. electrode gap distance.

4.2.1 12.5 μm Titanium-filtered PCD Energy

Energy calculated from the 12.5 μm Ti does not appear to follow any kind of fit. As seen in figure 4.5, no one material seems to scale up as cleanly as the hotspots did. This is likely due to the many shots that did not produce energy in the range of the Ti filter. Of all 136 shots, 57 of them did not produce a signal on the Ti-filtered PCD, effectively giving a reading of 0. This leads to very misleading averages for many of the gap distances.

However, we can still draw some meaningful conclusions from the energy

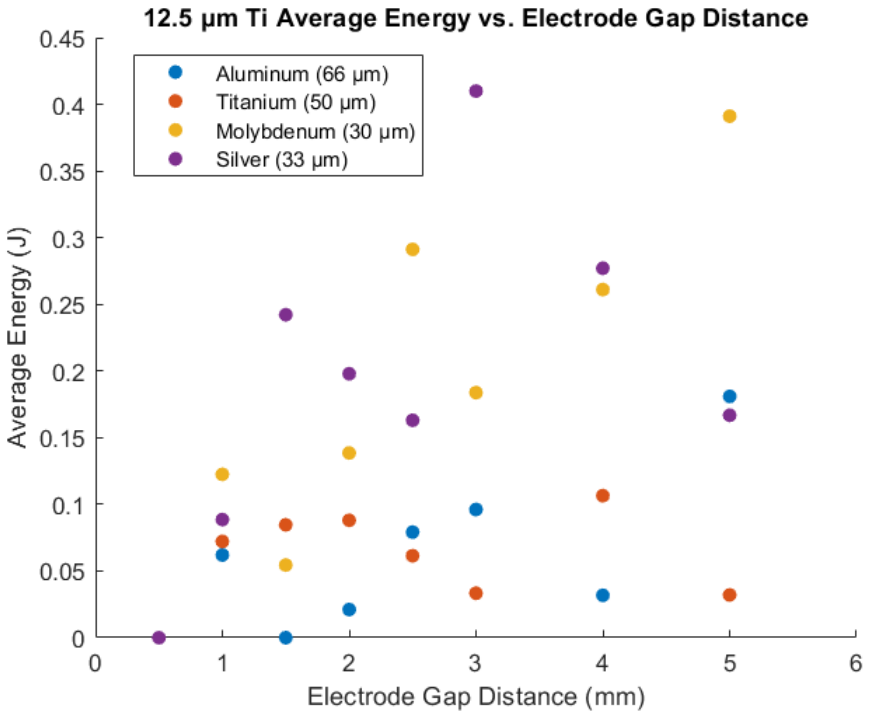

Figure 4.5: Plot of Titanium-filtered PCD Energy

A plot of the average peak energy reading from the Ti filtered diode against electrode gap distance for all four materials. Molybdenum and silver consistently produced more energy than the lower Z materials.

data. All 12 shots across all materials at 0.5 mm did not produce a peak, meaning no X-rays at 2-5 keV were recorded at the sensitivity used (oscilloscope sensitivity and distance from the source). On the other end, only 2 of the shots at 5.0 mm did not produce a peak. Furthermore, of the 57 shots that yielded no peaks, 22 were aluminum wire hybrid x-pinches while only 6 were with silver wire x-pinches. This data seems to imply that energy readings in the 2-5 keV range scales up with electrode gap distance and Z-numbers.

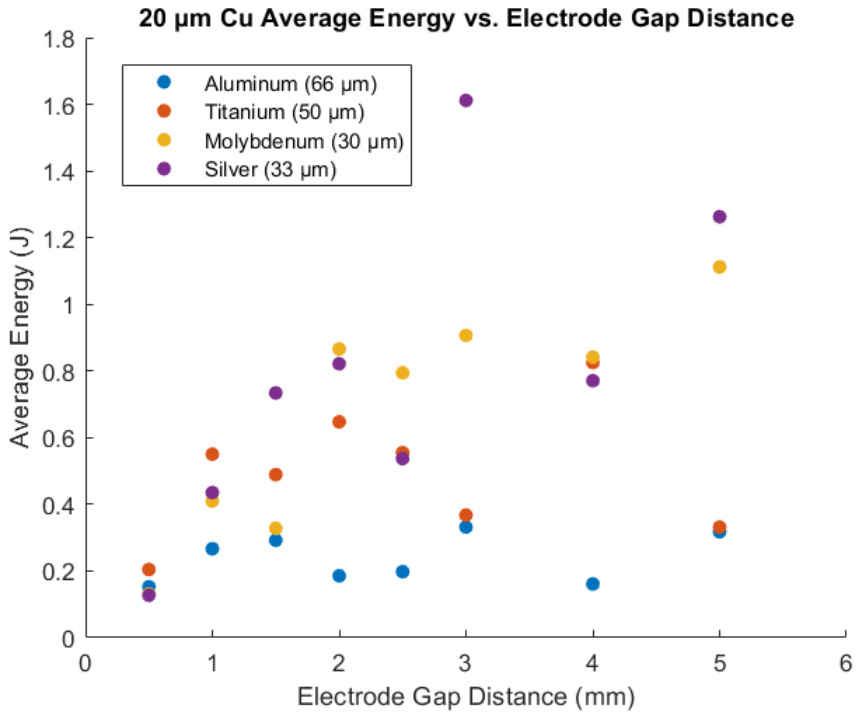

Figure 4.6: Plot of Copper-filtered PCD Energy

A plot of the average peak energy produced against electrode gap distance for all four materials. The aluminum shots consistently produced less energy compared to the other materials.

4.2.2 20 μm Copper-filtered PCD Energy

Data from the copper filtered diode yielded no readings without peaks. As with the hotspots, shots using molybdenum and silver produced higher readings in the 4-9 keV range than shots with aluminum and titanium at most gap distances. This is likely due to the electron beam radiation as peaks were often broader than those from the Ti PCD.

The copper filtered energy readings for each material scale slightly differently with electrode gap distance. Silver and titanium follow no real trend, with seemingly random jumps up and down as gap distance increases. Molybdenum has a more linear trend, with energy generally increasing with gap distance.

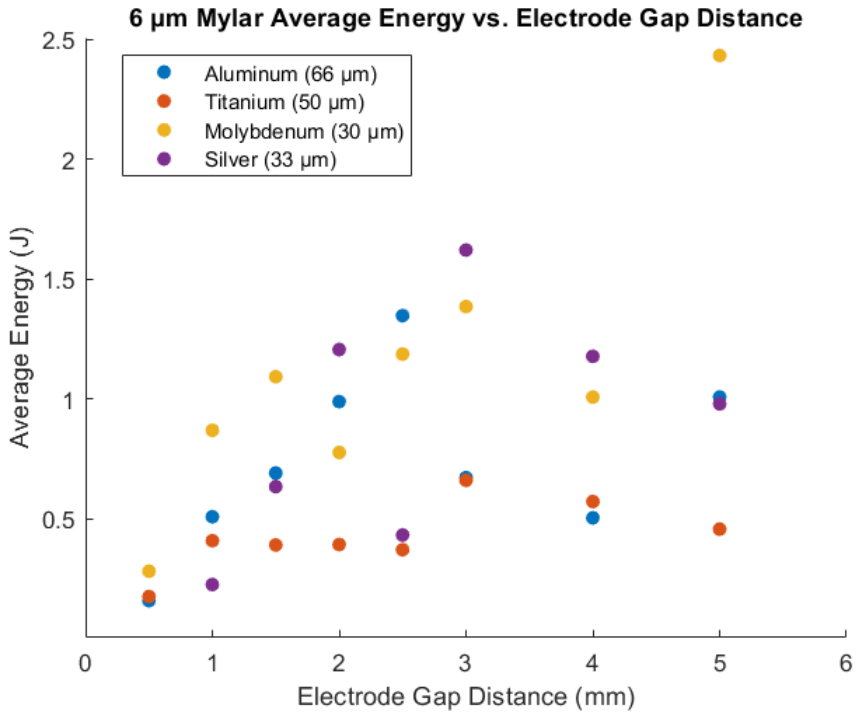

Figure 4.7: Plot of Mylar-filtered PCD Energy

A plot of the average peak energy produced against electrode gap distance for all four materials. Titanium produced the lowest energy readings compared to the other materials.

Aluminum's readings remains somewhat constant at all gap distances.

4.2.3 6 μm Mylar-filtered PCD Energy

The mylar filter allows the largest energy range through, giving the highest energy readings of the three filters. For the other two filters, lower energy photons were filtered out. This made the higher Z materials that produced the higher energies produce higher diode readings. With lower energy photons allowed through, aluminum shots produced higher readings than they did for the other two filters. For the Ti and Cu filters, the silver and molybdenum shots pro-

duced the highest energy readings. But for the mylar filter, the lower energy bound has aluminum shots producing higher energy readings for many of the gap distances. Titanium shots in general had the lowest energy readings.

Energy readings for aluminum, molybdenum, and sliver appear to scale up with electrode gap distance for the 0.5-3.0 mm electrode gap range. Each material has a few points that do not follow the upward trend, and the trend does not continue into the higher gap distances of 4-5 mm. Some of this could be due to statistical variation, as only three shots were taken at 4-5 mm compared to the 5 for the shorter gaps. Another possibility is electron beam-induced radiation for the higher Z materials producing higher energy readings. Titanium's energy readings appears to remain somewhat constant across the 1.0-2.5 mm range, and do not vary much at gap distances outside this range.

4.3 Source Size

Source size calculations were initially planned to be taken using images from the slit step wedge filter. However, due to the low magnification from the film canister, no detailed features of the peak were observed in any of the images. As such, a few extra shots were taken using a mesh and DR50 film as detailed in the Diagnostics section. These shots were taken using all four materials at 0.5 or 1.0 mm, as these were the best gap distances for producing one hotspot.

Of the 11 shots taken, 5 produced hotspots intense enough to produce an intensity plot clear enough to distinguish a slope to use for source size calculations. Mesh images produced penumbrae ranging from 3 to 8 pixels wide. This translates to source sizes between 2.7 and 7.1 μm. These numbers are probably

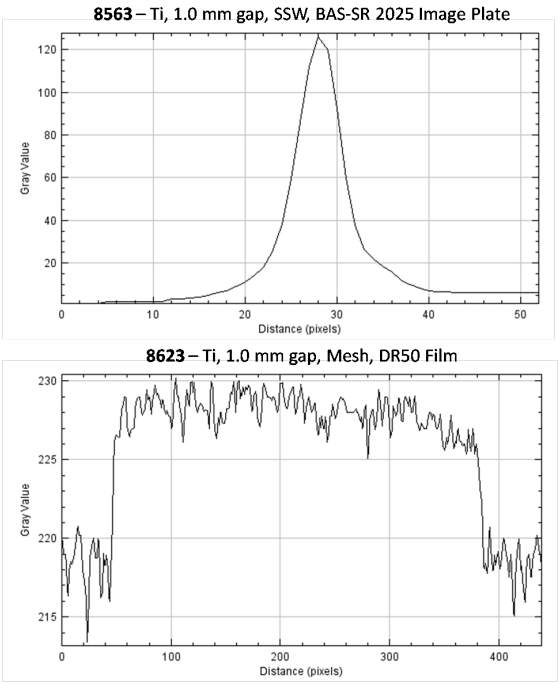

Figure 4.8: Image Plate and Film Comparison

The resolution difference between a SSW image on an image plate and a mesh image on a film is illustrated here. The difference in detail is due to both the higher magnification for the mesh (due to the geometry of the setup) and the higher dpi of the film. The higher detail in the mesh image enables more accurate source size calculation.

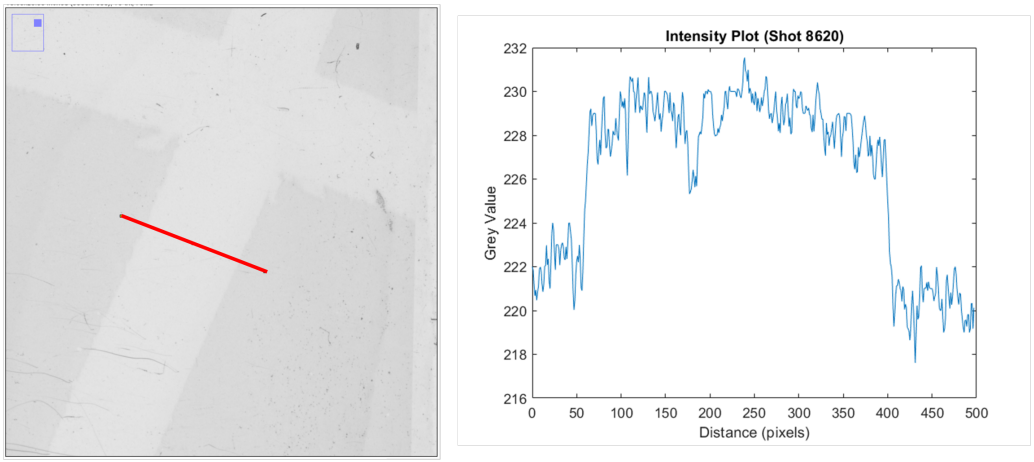

Figure 4.9: Intensity Plot for Source Size Calculation

An intensity plot of a mesh image generated by shot 8620, using aluminum wire at 0.5 mm gap distance. The slope is used to calculate the source size using equation 2.2. The wires in the mesh are 75 μm in diameter.

Shot	Material	Gap Distance (mm)	Fringe (pixels)	Source Size (μm)
8620	Al	0.5	5	4.4
8623	Ti	1.0	8	7.1
8625	Mo	1.0	6	5.3
8627	Ag	1.0	4	3.5
8628	Al	1.0	3	2.7

Table 4.1: Table of Shots used for Source Size Calculation

A table of the shots with a mesh that produced fringes clear enough to calculate the source size. The shots covered all materials at 1.0 mm and all produced sources smaller than 10 μm.

overestimates as these calculations are noramlly taken using 10-90% measurements rather than 0-100%. An ideal X-ray source would be around 1 μm, which was not achieved in this small set of shots. However, no large source sizes (> 10 μm) were generated, which is promising for the hybrid x-pinch setup. No real trend is apparent between materials or gap distances and with the much smaller sample size, no significant conclusions can be drawn based on different materials.

CHAPTER 5
CONCLUSION

This study set out to ascertain the connection between number of hotspots produced and variables such as electrode gap distance and wire material in hybrid x-pinch pulsed power experiments. These experiments showed all materials at higher gap distances produced more hotspots, with about 6 hotspots per shot at 4.0-5.0 mm. Meanwhile, shorter gap distances often produced a single hotspot, with an average of about 1.4 hotspots per shot at 0.5-1.0 mm. Additionally, shots at the higher gap distances had a higher variance in the number of hotspots produced, ranging between 4-12 hotspots per shot. The shorter gap distances produced a much smaller variance, with shots ranging between only 1-2 hotspots produced. Hotspot production scales with electrode gap distance differently for each material. Bearing in mind that there were only 5 shots per gap spacing, titanium and molybdenum scale very linearly, aluminum appears to increase in a stepwise manner, and silver has weak linear scaling.

Some weak trends can be seen in the energy and source sizes. Energy appears to scale up with electrode gap distance, though no real trend (linear or otherwise) is apparent. Higher Z materials (molybdenum and silver) produced higher energy readings than the lower Z materials (aluminum and titanium) for all three energy ranges viewed by the diodes, though this is likely due to electron beam radiation. Due to the low number of shots that were used to calculate source size, no real conclusions about electrode gap distance or wire material can be drawn. However, all shots using the mesh and high resolution film produced hotspots with a source size between 2.7 and 7.1 μm. The small source sizes are promising for the hybrid x-pinch setup.

APPENDIX A

APPENDIX

A.1 Number of Hotspots Log

Following are charts of each shot with details of the wire material, wire diameter, electrode gap distance, and hotspots generated. Also provided are the exact values for average energy as they appeared in the plots from the analysis section for data points that overlap.

A.1.1 Aluminum Series

Material	Diameter (µm)	Gap (mm)	Shot	Hotspots	Average
Aluminum	66	0.5	8600	1	1.33
			8601	2	
			8602	1	
		1.0	8603	1	1.40
			8604	1	
			8605	1	
			8606	2	
			8607	2	
		1.5	8595	1	1.40
			8596	1	
			8597	2	
			8598	2	
			8599	1	
		2.0	8432	3	3.00
			8433	3	
			8434	4	
			8446	2	
			8447	3	
		2.5	8537	4	3.20
			8574	3	
			8575	4	
			8590	2	
			8591	3	
		3.0	8492	5	5.00
			8493	4	
			8494	5	
			8496	6	
			8497	5	
		4.0	8587	4	4.67
			8588	5	
			8589	5	
		5.0	8592	8	6.33
			8593	6	
			8594	5	

A.1.2 Titanium Series

Material	Diameter (µm)	Gap (mm)	Shot	Hotspots	Average
Titanium	50	0.5	8576	1	1.33
			8577	1	
			8578	2	
		1.0	8561	2	1.60
			8562	1	
			8563	1	
			8564	2	
			8565	2	
		1.5	8556	3	2.00
			8557	2	
			8558	2	
			8559	2	
			8560	1	
		2.0	8551	2	2.60
			8552	3	
			8553	3	
			8554	2	
			8555	3	
		2.5	8538	3	3.40
			8539	2	
			8540	4	
			8541	3	
			8542	5	
		3.0	8543	3	4.00
			8544	4	
			8545	4	
			8546	5	
			8547	4	
		4.0	8548	4	5.00
			8549	5	
			8550	6	
		5.0	8566	8	6.33
			8567	6	
			8568	5	

A.1.3 Molybdenum Series

Material	Diameter (µm)	Gap (mm)	Shot	Hotspots	Average
Molybdenum	30	0.5	8582	1	1.00
			8583	1	
			8584	1	
		1.0	8509	1	1.20
			8510	1	
			8511	1	
			8512	1	
			8513	2	
		1.5	8504	2	1.60
			8505	1	
			8506	2	
			8507	0	
			8508	3	
		2.0	8441	3	3.60
			8442	4	
			8443	4	
			8444	4	
			8445	3	
		2.5	8498	4	4.20
			8499	2	
			8500	7	
			8502	5	
			8503	3	
		3.0	8454	3	4.60
			8455	7	
			8456	4	
			8457	5	
			8458	4	
		4.0	8514	6	5.67
			8572	5	
			8573	6	
		5.0	8569	12	7.67
			8570	5	
			8571	6	

A.1.4 Silver Series

Material	Diameter (µm)	Gap (mm)	Shot	Hotspots	Average
Silver	33	0.5	8579	2	1.33
			8580	1	
			8581	1	
		1.0	8525	2	1.80
			8526	2	
			8528	2	
			8529	2	
			8530	1	
		1.5	8520	2	3.40
			8521	4	
			8522	3	
			8523	4	
			8524	4	
		2.0	8448	4	4.00
			8449	5	
			8450	3	
			8451	4	
			8452	4	
		2.5	8515	5	4.40
			8516	4	
			8517	4	
			8518	5	
			8519	4	
		3.0	8459	3	4.40
			8460	4	
			8489	5	
			8490	4	
			8491	6	
		4.0	8531	7	7.67
			8532	9	
			8533	7	
		5.0	8534	4	5.00
			8535	4	
			8536	7	

A.1.5 Mesh Series

Shot	Material	Diameter (µm)	Gap (mm)	Hotspots
8619	Aluminum	66	0.5	1
8620	Aluminum	66	0.5	1
8621	Aluminum	66	1.0	1
8622	Titanium	50	0.5	1
8623	Titanium	50	1.0	2
8624	Molybdenum	30	0.5	1
8625	Molybdenum	30	1.0	2
8626	Silver	33	0.5	1
8627	Silver	33	1.0	1
8628	Aluminum	66	1.0	2
8629	Titanium	50	0.5	2
8630	Molybdenum	30	0.5	1

A.2 Energy Calculation Code

```
% Set and calculate constants
TiS = 9e-4;                 %Ti PCD sensitivity
spherer = 70;               %Radiative radius
APCD= .03;                  %PCD area
shot="08565";               %Shot number
MeshS = 3e-4;               %Mesh PCD sensitivity
Asphere = 4*pi*spherer^2; %Surface area of sphere
GF = Asphere/APCD;          %Geometric factor
IET=0;                      %Reset energy
K=0.8;                      %Energy threshold
Acheck=1;                   %Check total plot (true/false)
R = 50;                     %50 ohm
PCDr = 0.3;                 %PCD length

% Load data
data = load(strcat(shot,"_devC_Ti.txt"));
x = data(:,1);
y = data(:,2);

% Find peaks above K
[peaks,xloc]=findpeaks(y,'MinPeakHeight',K);

% Integrate under each peak and calculate energy
for n = 1:length(peaks)
    % integrating under the curve of interest
    V=trapz(x(xloc(n)-3:xloc(n)+3),y(xloc(n)-3:xloc(n)+3));

    % the radiation pattern is assumed to be isotropic
    E=(1/(R*TiS))*V;

    IET(n) = E*GF;
end

% Plot to check over
if Acheck==1
    plot(x,y)
else
    plot(x(xloc-3:xloc+3),y(xloc-3:xloc+3))
end
```

BIBLIOGRAPHY

[1] S.V. Lebedev, R. Aliaga-Rossel, S.N. Bland, J.P. Chittenden, A.E. Dangor, M.G. Haines, I.H. Mitchell. *The dynamics of wire array Z-pinch implosions*. The Blackett Laboratory, Imperial College. Physics of Plasmas Vol. 6 (no. 5), 2016-2022. 1998.

[2] T.W.L. Sanford, T.J. Nash, R.C. Mock, R.B. Spielman, K.W. Struve, J.H. Hammer, J.S. De Groot, K.G. Whitney, J.P. Apruzese. *Dynamics of a high-power aluminum-wire array Z-pinch implosion*. Sandia National Laboratories, Lawrence Livermore National Laboratory, Naval Research Laboratory. Physics of Plasmas Vol. 4 (no. 6), 2188-2203. 1997.

[3] S.V. Lebedev, F.N. Beg, S.N. Bland, J.P. Chittenden, A.E. Dangor, M.G. Haines, M. Zakaullah, S.A. Pikuz, T.A. Shelkovenko, D.A. Hammer. *X-ray backlighting of wire array Z-pinch implosions using X pinch*. The Blackett Laboratory, Imperial College, P.N. Lebedev Physical Institute, Laboratory of Plasma Studies. Review of Scientific Instruments Vol. 72 (no. 1), 671-673. 2000.

[4] D.B. Sinars, S.A. Pikuz, T.A. Shelkovenko, K.M. Chandler, D.A. Hammer. *Temporal parameters of the X-pinch x-ray source*. Laboratory of Plasma Studies, Cornell University. Review of Scientific Instruments Vol. 72 (no. 7), 2948-2956. 2001.

[5] F.S. Felber, N. Rostoker. *Kink and displacement instabilities in imploding wire arrays*. Maxwell Laboratories Inc., American Institute of Physics. The Physics of Fluids Vol. 24 (no. 6), 1049-1055. 1981.

[6] G.V. Ivanenkov, A.R. Mingaleev, S.A. Pikuz, V.M. Romanova, T.A. Shelkovenko. *Experimental Study of X-Pinch Dynamics*. Lebedev Institute of Physics, Russian Academy of Sciences. Plasma Physics Report Vol. 22 (no. 5), 363-378. 1995.

[7] T.A. Shelkovenko, S.A. Pikuz, A.D. Cahill, P.F. Knapp, D.A. Hammer, D.B. Sinars, I.N. Tilikin, S.N. Mishin. *Hybrid X-pinch with conical electrodes*. Laboratory of Plasma Studies at Cornell University, Sandia National Laboratories, Moscow Institute of Physics and Technology, P.N. Lebedev Physical Institute. Physics of Plasmas Vol. 17 (112707), 1-5. 2010.

[8] T.A. Shelkovenko, S.A. Pikuz, S.A. Mishin, A.R. Mingaleev, I.N. Tilikin, P.F. Knapp, A.D. Cahill, C.L. Hoyt, and D.A. Hammer. *Hybrid X-Pinches*.

P.N. Lebedev Physical Institute, Russian Academy of Sciences, Moscow Institute of Physics and Technology, Cornell University. Plasma Dynamics Vol. 38 (no. 5), 359-381. 2011.

[9] T.A. Shelkovenko, S.A. Pikuz, D.B. Sinars, K.M. Chandler, D.A. Hammer. *X Pinch Plasma Development as a Function of Wire Material and Current Pulse Parameters*. P.N. Lebedev Physical Institute, Sandia National Laboratories, Laboratory of Plasma Studies, School of Electrical and Computer Engineering, Cornell University. IEEE Transactions on Plasma Science Vol. 30 (no. 2), 567-576. 2002.

[10] T.A. Shelkovenko, S.A. Pikuz, D.A. Hammer, Y.S. Dimant, A.R. Mingaleev. *Evolution of the structure of the dense plasma near the cross point in exploding wire X pinches*. Laboratory of Plasma Studies, Cornell University. Physics of Plasmas Vol. 6 (no. 7), 2840-2846. 1999.

[11] T.A. Shelkovenko, I.N. Tilikin, G.V. Ivanenkov, W. Stepniewski, A.R. Mingaleev, V.M. Romanova, A.V. Agafonov, A.D. Cahill, C.L. Hoyt, P.A. Gourdain, D.A. Hammer, S.A. Pikuz. *Dynamics of Hybrid X-Pinches*. Lebedev Physical Institute, Russian Academy of Sciences, Institute of Plasma Physics and Laser Microfusion, Cornell University. Plasma Dynamics Vol. 41 (no. 1), 52-70. 2014.

[12] S.A. Pikuz, T.A. Shelkovenko, D.A. Hammer. *X-Pinch. Part I*. Lebedev Physical Institute, Russian Academy of Sciences, Cornell University. Plasma Physics Reports Vol. 41 (no. 4), 291-342. 2015.

[13] S.A. Pikuz, T.A. Shelkovenko, D.A. Hammer. *X-Pinch. Part II*. Lebedev Physical Institute, Russian Academy of Sciences, Cornell University. Plasma Physics Reports Vol. 41 (no. 6), 445-491. 2015.

[14] J.P. Chittendena, A.J. Power, M.G. Haines. *Further Investigations of Radiative Collapse in a Z-Pinch*. Blackett Laboratory, Imperial College. Plasma Physics and Controlled Fusion Vol. 31 (no. 11), 1813-1822. 1989.

[15] M.G. Haines. *An Analytic Model of Radiative Collapse of a Z-Pinch*. Blackett Laboratory, Imperial College. Plasma Physics and Controlled Fusion Vol. 31 (no. 5), 759-778. 1989.

[16] K.N. Koshelev, N.R. Pereira. *Plasma points and radiative collapse in vacuum sparks*. Institute for Spectroscopy, USSR Academy of Sciences, Berkeley Research Associates. Journal of Applied Physics Vol. 68 (no. 10), 21-44. 1991.

[17] Miyahara J. Imaging plate. In: Tateno Y., Iinuma T., Takano M. (eds) *Computed Radiography*. Springer, Tokyo. 1987.

[18] S.A. Pikuz, T.A. Shelkovenko, D.A. Hammer. *A Review of Projection Radiography of Plasma and Biological Objects in X-Pinch Radiation*. Lebedev Physical Institute, Russian Academy of Sciences, Cornell University. Plasma Physics Reports Vol. 42 (no. 3), 226-268. 2015.

[19] Carestream Health. *Kodak Industrex DR50 Film*. Quality NDE, Quebec. 2018.

[20] Byung Moo Song, Sergei A. Pikuz, Tatiania A. Shelkovenko, David A. Hammer. *Determination of the size and structure of an X-pinch x-ray source from the diffraction pattern produced by microfabricated slits*. Laboratory of Plasma Studies, Cornell University, P. N. Lebedev Physical Institute. Applied Optics Vol. 44 (no. 12), 2349-2358. 2005.

[21] I.N. Tilikin, T.A. Shelkovenko, S.A. Pikuz, D.A. Hammer. *Determination of the Size of a Radiation Source by the Method of Calculation of Diffraction Patterns*. Lebedev Physical Institute, Russian Academy of Sciences, Cornell University. Optics and Spectroscopy Vol. 115 (no. 1), 128-136. 2012.

[22] B.L. Henke, E.M. Gullikson, J.C. Davis. *X-ray interactions: photoabsorption, scattering, transmission, and reflection at E=50-30000 eV, Z=1-92*, Atomic Data and Nuclear Data Tables Vol. 54 (no.2), 181-342. 1993.

[23] T.A. Shelkovenko, S.A. Pikuz, C.L. Hoyt, A.D. Cahill, D.A. Hammer. *Hard X-rays from Hybrid X Pinches*. Cornell University, P.N. Lebedev Institute. AIP Conference Proceedings 1639, 108-111. 2014.